Asef controls vascular endothelial permeability and barrier recovery in the lung

[1]Xinyong Tian, [1]Yufeng Tian, [1]Grzegorz Gawlak, [1]Fanyong Meng, [2]Yoshihiro Kawasaki, [2]Tetsu Akiyama and [1]Anna A. Birukova

[1]Section of Pulmonary and Critical Care Medicine, Department of Medicine, University of Chicago, Chicago, Illinois 60637

[2]Laboratory of Molecular and Genetic Information, Institute for Molecular and Cellular Biosciences, The University of Tokyo, Bunkyo-ku, Tokyo 113-0032

Running title: Asef in endothelial barrier regulation

Keywords: GTPase, actin, permeability, cytoskeleton, pulmonary endothelium

Corresponding address:
Anna Birukova, MD
Lung Injury Center
Section of Pulmonary and Critical Care Medicine
Department of Medicine
University of Chicago
5841 S. Maryland Ave, MC-6026
Chicago, IL 60637
Phone: 773-834-2634
Fax: 773-834-2683
Email: abirukov@medicine.bsd.uchicago.edu

Supported by NIH NHLBI grants HL89257 and HL107920 and Grants-in-Aid for Scientific Research on Innovative Areas (Integrative Research on Cancer Microenvironment Network), MEXT, Japan.

ABSTRACT

Increased levels of hepatocyte growth factor (HGF) in the injured lungs may reflect compensatory response to diminish acute lung injury (ALI). HGF-induced activation of Rac1 GTPase stimulates endothelial barrier protective mechanisms. This study tested the involvement of Rac-specific guanine nucleotide exchange factor Asef in the HGF-induced endothelial cell (EC) cytoskeletal dynamics and barrier protection *in vitro* and in a two-hit model of ALI. HGF induced membrane translocation of Asef and stimulated Asef Rac1-specific nucleotide exchange

activity. Expression of constitutively activated Asef mutant mimicked HGF-induced peripheral actin cytoskeleton enhancement. In contrast, siRNA-induced Asef knockdown or expression of dominant negative Asef attenuated HGF-induced Rac1 activation evaluated by Rac-GTP pulldown and FRET assay with Rac1 biosensor. Molecular inhibition of Asef attenuated HGF-induced peripheral accumulation of cortactin, formation of lamellipodia-like structures, enhancement of VE-cadherin adherens junctions and compromised HGF protective effect against thrombin-induced RhoA GTPase activation, Rho-dependent cytoskeleton remodeling and EC permeability. Intravenous HGF injection attenuated lung inflammation and vascular leak in the two-hit model of ALI induced by excessive mechanical ventilation and thrombin signaling peptide TRAP6. This effect was lost in *Asef-/-* mice. This study shows for the first time the role of Asef in HGF-mediated protection against endothelial hyperpermeability and lung injury.

INTRODUCTION

The incidence of acute lung injury (ALI) in the US in 2011 was 129,320 cases per year (Blank and Napolitano, 2011). Despite protective ventilation strategies which decreased mortality by approximately 9%, the remaining 30-40% mortality rates (2000) continue to represent a serious threat. Therefore, better understanding of pathologic mechanisms driving ALI and equally important intrinsic mechanisms leading to restoration of lung function are needed for development of more efficient therapeutic approaches to confront ALI.

Clinical studies show dramatic (up to 25-fold) elevation of hepatocyte growth factor (HGF) levels in plasma and BAL fluid in patients with ALI/ARDS (Quesnel et al., 2008; Stern et al., 2000; Verghese et al., 1998). In addition to potential involvement in the alveolar epithelial repair process in the lung (Ware and Matthay, 2002), HGF promotes cell survival and enhancement of lung endothelial barrier properties critical for restoration of lung vascular barrier function (Birukova et al., 2007a; Liu et al., 2002; Matsumoto and Nakamura, 1996). These observations suggest that endogenous repair mechanisms, such as HGF elevation, exist to provide essential signals for lung recovery. Our group has previously shown HGF-induced activation of Rac1-GTPase, which leads to endothelial barrier protection via enhancement of the peripheral actin cytoskeleton (Birukova et al., 2007a; Liu et al., 2002). However, the upstream mechanism of Rac1 activation by HGF remains unclear.

Rac1 GTPase acts as a molecular switch, cycling between the active GTP-bound and the inactive GDP-bound state which is regulated by guanine nucleotide exchange factors (GEFs) facilitating exchange of GDP for GTP, GTPase-activating proteins (GAPs), which increase the intrinsic rate of GTP hydrolysis by Rac1 GTPase, and by guanine nucleotide dissociation inhibitors (RhoGDI) which associate with inactivated Rac (Bishop and Hall, 2000; Boguski and McCormick, 1993; Zheng, 2001). Rac1 promotes EC barrier properties by stimulating peripheral actin polymerization and cortical actin cytoskeletal dynamics, re-annealing the disrupted intercellular adherens junctions, formation of adherens junction-associated signaling protein complexes, and

downregulation of barrier disruptive Rho GTPase signaling (reviewed in (Birukov et al., 2013)). Thus, molecular mechanisms which precisely control the balance between Rho- and Rac1 signaling are essential for EC barrier regulation in physiologic and pathologic conditions.

Asef is a Rac1-specific GEF which contains Dbl homology (DH) domain exhibiting guanine nucleotide exchange (GEF) activity, plekstrin homology (PH) domain which determines the subcellular localization and activity by interacting with phosphatidylinositol phosphate, and Src homology 3 (SH3) autoinhibitory domain and a region that binds tumor suppressor protein APC (APC domain) (Kawasaki et al., 2003). Asef has been proposed to regulate the actin cytoskeleton in epithelial and neuronal cells by activating Rac1 and Cdc42 GTPases (Kawasaki et al., 2000). Constitutive Asef activation by truncated APC in colorectal tumor cells caused decreased cell-cell adhesion and aberrant migratory phenotypes (Kawasaki et al., 2013), while overexpression of Asef decreased E-cadherin-mediated cell-cell adhesion and promoted migration of kidney epithelial cells (Kawasaki et al., 2003). The role of Asef in vascular endothelial barrier regulation at present is unknown.

This study used several complementary approaches including biochemical assays, live imaging, molecular inhibition approaches to investigate the role of Asef in control of lung endothelial barrier and HGF-induced vascular barrier protection. Using a genetic animal model, we evaluated the role of Asef in the two-hit animal model of acute lung injury. Asef-dependent mechanisms of Rac1

activation and HGF-induced endothelial barrier protection were linked to the downregulation of the barrier-disruptive Rho pathway.

RESULTS

HGF-induced activation of Asef triggers Rac1 signaling. The HGF-induced endothelial barrier protective response is associated with activation of Rac1 GTPase signaling, but precise mechanisms of Rac1 activation remain elusive. We found that HGF induced activation of Rac1 (**Figure 1A**) which was associated with rapid stimulation of Asef nucleotide exchange activity towards Rac1 observed at 2 - 10 min after HGF addition (**Figure 1B**). Western blot analysis showed comparable levels of Asef expression in both human lung microvascular and pulmonary artery EC cultures. These data suggest the role for Asef-dependent signaling mechanisms in EC from different vascular beds. HGF-induced activation of Asef guanine nucleotide exchange activity towards Rac1 was abrogated by cell pretreatment with pharmacologic inhibitor of HGF receptor c-Met (**Figure 1C**). Activation of Asef by HGF also led to Asef translocation to the cell membrane fraction (**Figure 1D**) with preferential accumulation at the cell periphery visualized by immunofluorescence staining with Asef antibody (**Figure 1E**).

Molecular inhibition of Asef in pulmonary EC using siRNA-mediated knockdown delayed establishment of endothelial monolayers monitored by measurements of transendothelial electrical resistance (TER) (**Figure 2A**). Using the Rac1 FRET biosensor (Birukova et al., 2012) we evaluated the time course of

regional Rac1 activation in subconfluent pulmonary EC cultures. HGF induced rapid activation of Rac1 (**Figure 2B**), while Asef knockdown significantly suppressed the HGF-induced Rac1 activation. The quantitative analysis of FRET data is summarized in **Figure 2C**. Because this study investigated the ability of HGF to restore endothelial monolayer integrity, the sub-confluent EC cultures were used in the following experiments. Asef knockdown abolished HGF-induced Rac1 activation, monitored by Rac-GTP pulldown assay (**Figure 2D**). To test if Asef-mediated Rac1 activation is additionally regulated by cell-cell contacts, HGF-induced Rac1 activity was also evaluated in sparse (**Figure 2E**) and dense (confluent) (**Figure 2F**) EC cultures. Representative phase contrast microscopy images in Figures 2DEF depict cell density of HPAEC cultures used in these experiments, although actual densities could slightly vary between experiments. HGF activated Rac1 GTPase at all three cell density conditions, and the effect was abolished by Asef knockdown.

Asef mediates dynamic peripheral cytoskeletal remodeling in HGF-stimulated EC. Several actin-binding proteins including the Arp2/3 complex, p21Arc, PAK1 and cortactin, control peripheral actin polymerization and cortical actin structure (Borisy and Svitkina, 2000; Weed and Parsons, 2001). Cortactin is an actin-binding activator of peripheral actin polymerization (Uruno et al., 2001). Translocation of cortactin to the cell periphery is mediated by Rac1 and blocked in cells with inhibited Rac1 activity (Weed et al., 1998). Rac1 activation is also required for cortactin tyrosine phosphorylation and activation of actin cytoskeletal

dynamics such as membrane ruffling and lamellipodia formation (Ammer and Weed, 2008; Head et al., 2003; Vouret-Craviari et al., 2002). Involvement of Asef in the HGF-induced peripheral cytoskeletal dynamics was first evaluated by analysis of cortactin membrane translocation, which indicates cortactin activation (Dudek et al., 2004; Uruno et al., 2001). HGF stimulated cortactin translocation to the membrane fraction; this effect was attenuated by Asef knockdown (**Figure 3A**). Rac1 activation triggers signaling pathways leading to increased cortactin tyrosine phosphorylation (Head et al., 2003). Indeed, we observed the HGF-induced increase in cortactin phosphorylation at Tyr^{421} which was markedly attenuated by Asef knockdown (**Figure 3B**).

The Asef-dependent mechanism of HGF-induced activation of peripheral actin cytoskeletal dynamics was further examined in experiments with the live imaging of GFP-tagged cortactin. HGF induced rapid formation of cortactin-positive lamellopodia-like structures which were observed as early as 2 min and remained prominent during the 30-min observation period (**Figure 3C, top panels**). In contrast, Asef knockdown abolished HGF-induced activation of peripheral cytoskeletal remodeling (**Figure 3C, bottom panels**). Insets in Figure 3C depict phase contrast microscopy images of tested cells. Collectively, these results demonstrate a critical role of Asef in the activation of cortical cytoskeletal dynamics via stimulation of Rac1 cytoskeletal effectors.

Potential effect of EC confluence on Asef-dependent peripheral cortactin activation and actin cytoskeletal remodeling was further tested. Activation of cortactin in response to HGF was reflected by cortactin phosphorylation and

accumulation in cell peripheral lamellipodia-like structures and was observed in both, sparse and dense EC monolayers (**Figure 3DE**). These effects were markedly attenuated by Asef knockdown in both, sparse and dense EC cultures. Cortactin translocation was also accompanied by increased F-actin accumulation at cell peripheral compartments (**Figure 4A**). Inspection of subcortical F-actin accumulation at different cell regions revealed that HGF-induced cortical F-actin accumulation in lamellipodia-like structures was observed in the regions with intercellular gaps (**inset-1 in Figure 4A**), but also in the regions of established cell-cell contacts (**inset-2 in Figure 4A** and **Figure 4B**). HGF-induced cortical actin dynamics was inhibited by Asef knockdown (**Figure 4AB**). These data show that HGF-induced Asef activity stimulates cortical cytoskeletal dynamics in a cell contact-independent manner.

Asef mediates HGF-induced endothelial barrier enhancement. The role of Asef in the HGF-induced EC barrier enhancement was further investigated in the functional tests using measurements of transendothelial electrical resistance (TER). Confluent human pulmonary EC grown on the gold microelectrodes for TER measurements were transfected with Asef-specific siRNA duplexes. Control cells were transfected with non-specific RNA. The basal TER levels were not affected by Asef knockdown (data not shown). Asef depletion significantly attenuated HGF-induced EC barrier enhancement monitored by diminished TER increase in a dose-dependent manner (**Figure 4C**).

The effects of Asef knockdown on HGF-induced EC barrier enhancement were further tested using visualization of local areas in the EC monolayers with increased EC permeability for macromolecules (**Figure 4D**). In control conditions, some accumulation of FITC-labeled tracer at sites underlying the cell-cell junction area was observed. These results reflect the basal level of mass transport across the cell-cell junction area in EC monolayers. HGF significantly decreased the basal EC monolayer permeability for FITC-labelled avidin (**Figure 4D, bottom left panel**). Barrier enhancing effect of HGF was abrogated in EC monolayers with Asef knockdown (**Figure 4D, bottom right panel**).

Modulation of Asef activity affects HGF-induced peripheral cytoskeletal enhancement. As a complementary approach to experiments with Asef knockdown, we performed ectopic expression of HA-tagged wild type Asef or its constitutively activated (CA-Asef) or dominant negative (DN-Asef) mutants (Kawasaki et al., 2003). Overexpression of wild type Asef further enhanced EC peripheral actin remodeling in response to HGF in comparison to HGF-stimulated non-transfected cells (**Figure 5A**). In turn, expression of activated Asef mutant in non-stimulated cells reproduced peripheral actin cytoskeletal rearrangement observed in non-transfected EC treated with HGF (**Figure 5B**). Similarly to Asef knockdown experiments, the expression of dominant negative Asef abrogated HGF-induced formation of lamellipodia-like structures and peripheral actin rim (**Figure 5C**). Expression of dominant negative Asef mutant suppressed the HGF-induced activation of Rac1 GTPase in pulmonary EC (**Figure 5D**).

Adherens junction formation in HGF-stimulated HPAEC is cell density-dependent and controlled by Asef. VE-cadherin accumulation at the cell membrane compartment is essential for initiation adherens junction protein complex assembly. Using subcellular fractionation assay, we examined VE-cadherin membrane translocation in confluent (**Figure 6A**) and sparse (**Figure 6B**) EC cultures after HGF-stimulation. HGF induced robust VE-cadherin membrane accumulation in dense (confluent) EC monolayers, but not in sparse EC cultures. Observed VE-cadherin membrane accumulation was significantly attenuated in HGF-stimulated EC with Asef knockdown. Immunofluorescence staining of VE-cadherin shows dramatic increase of VE-cadherin-positive immunofluorescent signal at the cell junction area of HGF-stimulated EC monolayers. This effect was abolished by Asef knockdown (**Figure 6C**).

Next, we tested the role of Asef in regulation of interaction between VE-cadherin and its adherens junction binding partner p120-catenin. HPAEC with depleted Asef or control cells were stimulated with HGF, and VE-cadherin - p120-catenin interactions were tested by reciprocal co-immunoprecipitation assays using VE-cadherin or p120-catenin antibodies. HGF treatment of control EC further increased interaction between VE-cadherin and p120-catein, which was suppressed in Asef-depleted cells (**Figure 6D**). These data suggest Asef-dependent mechanism of HGF-induced assembly of VE-cadherin adherens junction protein complex and link these effects with EC barrier enhancement.

Asef mediates protective effect of HGF against thrombin-induced EC permeability. Agonist-induced activation of Rac1 protects the vascular endothelial barrier in thrombin-stimulated EC by inhibiting the thrombin-induced Rho pathway of barrier dysfunction (Baumer et al., 2009; Birukova et al., 2007c; Finigan et al., 2005; Tauseef et al., 2008). Involvement of Asef in the HGF-induced barrier protective effects against thrombin was tested in control and Asef-depleted cells. Agonist-induced permeability responses in control cells treated with non-specific RNA and Asef-depleted EC monolayers were monitored by TER measurements. HGF exhibited the prominent protective effect against thrombin-induced TER decline in EC monolayers treated with non-specific RNA (**Figure 7A, left panel**). In contrast, Asef knockdown impaired HGF-induced EC barrier protection against thrombin (**Figure 7A, right panel**). Effects of Asef knockdown on agonist-induced TER changes are summarized in the bar graph in **Figure 7A (lower panel**).

The role of Asef in the HGF-induced preservation of EC monolayer integrity was further examined by immunofluorescence studies. Control and Asef-depleted EC were challenged with thrombin with or without HGF pretreatment. Thrombin induced rapid formation of stress fibers and intercellular gaps which was observed in both, control and Asef-depleted EC monolayers (**Figure 7B**). HGF partially preserved the integrity of thrombin-challenged EC monolayers treated with nonspecific RNA, but this protective effect was lost in EC with depleted Asef.

The Rho pathway of endothelial permeability involves phosphorylation of myosin-binding subunit of myosin-associated phosphatase type 1 (MYPT1) at the Rho kinase specific site Thr-850 (Essler et al., 1998; Velasco et al., 2002) leading to increased myosin light chain (MLC) phosphorylation and activated actomyosin contraction. We examined effects of HGF and thrombin on Rho activation (**Figure 7C**) and MYPT1 and MLC phosphorylation levels (**Figure 7D**) in control and Asef-depleted cells. Thrombin stimulation strongly activated Rho and increased MYPT1 and MLC phosphorylation in both control cells and cells with Asef knockdown. However, attenuation of thrombin-induced Rho signaling by HGF pretreatment was observed in control HGF- and thrombin-treated EC, but not in EC with Asef knockdown.

Asef mediates protective effects of HGF in the two-hit model of lung injury.

The studies in pulmonary EC culture described above demonstrate a critical role for Asef as a key mediator of HGF-induced Rac1 signaling leading to activation of peripheral actin cytoskeletal dynamics and endothelial barrier enhancement, as well as attenuation of Rho-dependent barrier disruptive mechanisms. Development of ventilator-induced lung injury (VILI) is a complex process triggered by pathologic mechanical forces acting on lung tissue and accompanied by elevation of circulating proinflammatory cytokines and mediators (IL-8, IL-1β, coagulation proteins, etc.). Based on these findings, a two-hit (or even multiple hit) animal model of VILI has been accepted by scientific community to better represent the clinical manifestations of acute lung injury

(Matthay et al., 2003). The role of Asef in vascular protective effects of HGF was further investigated in the two-hit model of lung injury previously characterized by our group (Birukova et al., 2010; Birukova et al., 2011), which was induced by mechanical ventilation at high tidal volume (HTV, 30 ml/kg) combined with intravenous injection of thrombin related activating peptide (TRAP6), the thrombin-derived non-thrombogenic peptide that serves as a PAR1 receptor ligand (Storck and Zimmermann, 1996).

Asef-/- mice and matching *Asef+/+* controls were injected with vehicle or HGF prior to challenge with TRAP6 and mechanical ventilation. Evaluation of the bronchoalveolar lavage (BAL) after 4 hours of TRAP6/HTV revealed a significant elevation of BAL protein content reflecting lung barrier dysfunction in both the *Asef+/+* and *Asef-/-* mice (**Figure 8A**). However, HGF protective effects against TRAP6/HTV-induced increases in BAL protein content observed in *Asef+/+* controls were abolished in *Asef-/-* mice. TRAP6/HTV-induced lung injury caused significant lung vascular leak detected by Evans blue dye accumulation in the lung parenchyma, which was evident in *Asef+/+* and *Asef-/-* mice after 4 hours of HTV. In turn, pre-treatment with HGF caused a substantial decrease in Evans blue accumulation in the *Asef+/+* mice, but not in *Asef-/-* mice. Images of original lung preparations showing Evans blue extravasation are shown in **Figure 8B**. Quantitative analysis of Evans blue-labeled albumin in the lung tissue extracts from these experiments is presented in **Figure 8C**.

Exposure to TRAP6/HTV also significantly increased the total cell and neutrophil count in BAL samples in both the *Asef+/+* and *Asef-/-* mice, as

compared to the non-ventilated controls (**Figure 9A**). Although we observed a trend towards higher levels of BAL cell count in TRAP6/HTV-treated *Asef-/-* mice, it did not reach statistical significance. By contrast, HGF administration prior to TRAP6/HTV caused significant reduction of cellular infiltration in *Asef*+/+ mice, but not in *Asef-/-* mice. TRAP6/HTV caused a significant increase in lung MPO activity compared with the control group (**Figure 9B**). HGF decreased MPO activity in the lungs of TRAP6/HTV-exposed *Asef*+/+ mice, while in the *Asef-/-* mice this effect was statistically insignificant.

Histological analysis of lung sections showed that TRAP6/HTV induced inflammatory cell infiltration (predominantly neutrophils and mononuclear cells) in both lung interstitium and alveolar compartments of *Asef*+/+ and *Asef-/-* mice (**Figure 9C**). Pretreatment with HGF markedly attenuated TRAP6/HTV-induced inflammatory cell infiltration in lung tissue of *Asef*+/+ mice, but failed to induce comparable protective effects in *Asef-/-* mice.

DISCUSSION

Alterations in vascular permeability are the defining feature of several diverse processes, including inflammation, ischemia/reperfusion, and ventilator-induced lung injury. Increased endothelial permeability causes alveolar flooding, hypoxemia, and tissue leukocyte infiltration, which triggers inflammatory cytokine production and may lead to increased morbidity and mortality. Increased levels of circulating HGF have been observed in experimental models and in patients with acute lung injury and ARDS syndrome (Geiser, 2003; Ware and Matthay, 2002). Importantly, HGF upregulation by pathogenic stimuli has been linked to

pulmonary recovery after pathological insult (Geiser, 2003; Ware and Matthay, 2002) suggesting that HGF may serve as a protective agonist in lung reparative processes and in restoration of vascular permeability to normal levels. However, molecular mechanisms underlying effects of HGF on pulmonary EC barrier restoration are not yet well-understood.

This study shows for first time the role of Asef in the HGF-induced establishment of EC monolayer integrity and Asef-dependent regulation of agonist-induced vascular endothelial permeability. HGF-induced Asef activation triggered activation of Rac1 and stimulated peripheral actin cytoskeletal dynamics in the pulmonary endothelium, which is a key mechanism of endothelial integrity restoration. Peripheral localization of Asef in the HGF-stimulated cells suggested local activation of Rac1 signaling also critical for re-establishment of cell-cell junction complexes (Arthur et al., 2002; Birukova et al., 2012; Noren et al., 2001) and further enhancement of EC barrier.

To further elucidate these mechanisms, we performed additional studies in sparse, sub-confluent and confluent EC cultures exposed to HGF. The results show that cell seeding density and cell contact state did not impair Asef-mediated Rac1 signaling and activation of cortical actin cytoskeletal dynamics induced by HGF. Interestingly, the data showed that Asef mediates HGF-induced formation of lamellipodia-like structures even in confluent EC monolayers with established cell-cell junctions. In contrast, HGF-induced, Asef-dependent VE-cadherin membrane translocation and VE-cadherin association with p120-catenin was detected in confluent EC monolayers, but not in sparse EC cultures. These

results suggest that HGF-induced establishment of EC intercellular junctions is mediated by Asef, but requires cell contacts formed by HGF-stimulated expanding cells. Altogether, these data provide a compelling evidence for the Asef role in the HGF-induced re-establishment of EC monolayer integrity and barrier properties via two complementary mechanisms: activation of peripheral actin cytoskeletal dynamics leading to cell extension and closing gaps in a monolayer, and formation of cell-cell contacts, where Asef stimulates establishment of the specialized junctional structures.

Restoration of EC integrity and cell junctions also requires local downregulation of Rho signaling (Anastasiadis et al., 2000). Our previous studies described the mechanism of local Rho inhibition via Rac1-mediated activation of Rho-specific negative regulator, p190RhoGAP, and its recruitment to adherens junctions by p120-catenin (Birukova et al., 2011; Zebda et al., 2013) leading to enhancement of cortical actin, disappearance of central stress fibers and EC barrier enhancement. Dissolution of central stress fibers due to Rho inactivation and activation of cortical actin remodeling and cell junctions in endothelial cells stimulated with Rac1-activating agonists is well recognized (Birukov et al., 2004; Dudek et al., 2004; Fukuhara et al., 2005; Garcia et al., 2001), and p190RhoGAP-dependent Rho inactivation discussed above is one of several potential mechanisms of HGF-induced suppression of Rho activity. Other mechanisms of negative Rho regulation by HGF-induced Rac1 signaling may include direct interaction of Rac1 with Rho inhibitor RhoGDI (Stultiens et al., 2012), inhibition of the low-molecular-weight protein tyrosine phosphatase,

leading to activation of p190RhoGAP (Nimnual et al., 2003), or downregulation of Rho-specific guanine nucleotide exchange factors and resulting in reduction of the RhoGTP pool. For example, recent study has described HGF-induced microtubule growth (Tian et al., 2014), which may lead to capturing and inactivation of MT-interacting Rho-specific GEF-H1. Detailed mechanisms of Asef-dependent Rac1-Rho crosstalk in HGF-stimulated endothelium await further investigation. It is also possible that HGF-induced activation and accumulation of Asef at the cell junction area observed in this study promotes EC barrier restoration by triggering Rac1-dependent recruitment to cell periphery and activation of p190RhoGAP. This intriguing possibility warrants further investigation.

In addition to Asef described in this study, another Rac1-specific GEF, Tiam1 was also implicated in HGF protective effects (Birukova et al., 2007a; Singleton et al., 2007). Nucleotide exchange activity of Tiam1, which mediates HGF-induced Rac1 activation and EC barrier protective response, can be regulated by diverse mechanisms, including phosphorylation by tyrosine kinases, Ca^{2+}/calmodulin–dependent kinase II (CaMKII) or related kinases, interaction with PI3-kinase product PtdIns(3,4,5)P_3, binding to cell surface molecule CD44 or cytoskeletal protein ankyrin, as well as direct binding to activated Ras (Servitja et al., 2003; Welch et al., 2003; Zheng, 2001). Signaling mechanisms regulating Asef activity are not yet completely understood. Since Asef and Tiam1 may be regulated by different mechanisms, our present and published data suggest the certain overlap of GEFs in HGF-induced Rac1 activation, but do not exclude

different mechanisms of Tiam1 and Asef activation by HGF or other barrier enhancing molecules.

This study demonstrates for the first time a major role of Asef in the lung barrier protection in the two-hit animal model of acute lung injury. Absence of Asef is compatible with normal physiologic functioning of mice, and we did not observe any noticeable changes in the basal levels of BAL protein, cell counts or alterations in lung histology (data not shown). However, Asef ablation caused nearly complete inhibition of Rac1 activation in response to VEGF and bFGF in cells isolated from *Asef-/-* mice leading to impaired cell migration and tube formation, although expression of other Rac-specific GEFs was not affected (Kawasaki et al., 2011). On the other hand, our results show significant attenuation of barrier protective and anti-inflammatory effects of HGF in the TRAP6/HTV model of lung injury.

Although Asef expression by the alveolar epithelial cells was not analyzed in this study, Asef expression by epithelial cells derived from other beds has been reported (Cheng et al., 2013; Kawasaki et al., 2009). Therefore, in experiments with global Asef knockout, we cannot exclude a potential impact of other cell types, such as alveolar type I epithelium in the HGF protective effects. Evaluation of potential Asef role in control of alveolar epithelial barrier requires further investigation. On the other hand, measurements of vascular permeability *in vivo* (Figure 8) suggest a critical involvement of lung vascular endothelium in the Asef-dependent HGF-mediated protection against ventilator-induced acute lung injury.

In summary, this study shows that HGF promotes enhancement of lung endothelial barrier properties critical for restoration of vascular barrier function. Activation of Asef-Rac-dependent lung vascular barrier restoration may represent an autoregulatory mechanism directed at downregulation of barrier disruptive signaling and resolution of pathologic conditions. The results of this study also suggest that targeted activation of Rac1-specific GEFs such as Asef may accelerate endothelial barrier recovery and promote resolution of lung injury.

MATERIALS AND METHODS

Cell culture and reagents. Human pulmonary artery endothelial cells (HPAEC) were obtained from Lonza (East Rutherford, NJ) and used for experiments at passages 5-7. Subconfluent HPAEC cultures were plated at 260 cells/mm^2 density and grown for 48 hours to reach 70-80% confluence. To achieve sparse and completely confluent cell monolayers, HPAEC were plated at 150 cells/mm^2 and 600 cells/mm^2 densities, respectively. In studies with thrombin model of endothelial disruption, the cells were grown for 72 hours to reach 100% confluence (600-700 cells/mm^2). In experiments with DNA transfections, the cells were plated at 30-40 % density, transfected next day and analyzed after 24 hours of transfection. In experiments with siRNA transfections, the cells were plated at 30-40 % density, transfected next day, grown for 48 hours, then replated at lower density and analyzed after 24 hours (total transfection time 72 hours). For TER measurements, the cells were grown for 72 hours after transfection without replating. Plasmids encoding HA-tagged wild type Asef, dominant negative Asef$^{\Delta DH}$ and constitutively active Asef$^{\Delta APC}$ mutants subcloned into pcDNA3.1

(Invitrogen, Carlsbad, CA) have been described elsewhere (Kawasaki et al., 2003). Human HGF was obtained from R&D Systems (Minneapolis, MN). Cell-permeable c-Met kinase inhibitor, N-(3-Fluoro-4-(7-methoxy-4-quinolinyl)phenyl)-1-(2-hydroxy-2-methylpropyl)-5-methyl-3-oxo-phenyl-2,3-dihydro-1H-pyrazole carboxamide, was purchased from Millipore (Billerica, MA). Texas Red-conjugated phalloidin and Alexa Flour 488 were purchased from Molecular Probes (Eugene, OR). Asef, Rac1, RhoA and HA-tag antibodies were purchased from Santa Cruz Biotechnology (Santa Cruz, CA); cortactin and phospho-Tyr^{421} cortactin antibodies were from Millipore (Billerica, MA); and HRP-linked anti-mouse IgG, di-phospho-MLC and phospho-MYPT antibodies were obtained from Cell Signaling Inc. (Beverly, MA). Unless otherwise specified, all biochemical reagents, including β-actin antibodies, were obtained from Sigma (St. Louis, MO).

Asef knockdown in human pulmonary EC culture. To deplete endogenous Asef, a Asef-specific set of three Stealth™ Select siRNA duplexes was purchased from Invitrogen (Carlsbad, CA) in ready-to-use, desalted, deprotected, annealed double-strand form. Non-specific RNA (Dharmacon, Lafayette, CO) was used as a control treatment. Transfection of EC with siRNA was performed as previously described (Birukova et al., 2010). After 72 hours of transfection, cells were used for experiments or harvested for western blot verification of specific protein depletion.

GTPase and GEF activation assays. Rac1 and RhoA activation was evaluated in pulldown assays using agarose beads with immobilized PAK1-PBD and rhotekin-RBD, respectively (Birukov et al., 2004). In brief, after stimulation, cell lysates were collected, and GTP-bound Rac1 or Rho were captured using pull-down assays with immobilized PAK1-PBD or Rhotekin-RBD, respectively. The levels of activated small GTPases as well as total Rac1 and Rho content were evaluated by western blot analysis. Active Asef was affinity precipitated from cell lysates according to previously described protocol (Waheed et al., 2013) using the Rac1 (G15A) mutant which cannot bind nucleotide and therefore has high affinity for activated GEFs (Garcia-Mata et al., 2006). Activated Asef in Rac1 (G15A) pulldowns was detected by Western blotting and normalized to total Asef in cell lysates for each sample. Precipitation with glutathione–Sepharose beads containing no fusion proteins resulted in no Asef precipitation.

Fluorescent resonance energy transfer (FRET). The Rac1-FRET biosensor was kindly provided by Yingxiao Wang (University of Illinois at Urbana-Champaign, IL). FRET analysis was performed as described elsewhere (Birukova et al., 2012; Poh et al., 2009). Cells were seeded on Matek glass-bottom dish coated with gelatin. 24 hours after transfection, medium was changed to 2% FBS EBM medium for 2 hour. For detection of FRET, the cells were maintained on the microscope stage at 37 °C. To minimize the photobleaching effect, the time interval for each imaging acquisition was set to be 30 s, and images were captured for 10 min using Olympus Model IX71

Microscope System equipped with a 60X oil immersion objective and a CCD camera. Metamorph software was used to control the filter wheel and data analysis. The ratiometric images of ECFP/YPet were computed and generated by the Metamorph software to represent the spatiotemporal FRET signals. Analysis of regional Rac1 activation was performed using integral ECFP/YPet values in ~ 5 μm wide areas at the cell periphery and equal areas in the central parts of the cell. Increased Rac1 activation (ECFP/YPet emission ratio) at the cell periphery was normalized to Rac1 activation in central parts of the cell and expressed as bar graphs. Comparisons were made between un-stimulated cells and cells stimulated with HGF (6 min) with and without Asef depletion.

Live imaging of cells expressing GFP-cortactin. Cells were plated on MatTek dishes (MatTek, Ashland, MA) and transfected with GFP-cortactin. Images were acquired with 100x NA 1.45 oil objective in a 3I Marianas Yokogawa-type Spinning Disk Confocal system equipped with a CO_2 chamber and a heated stage. Time lapse images were taken with 2 second intervals for 30 min.

Immunofluorescence. Endothelial monolayers plated on glass cover slips were treated with the agonist of interest, fixed in 3.7% formaldehyde solution in PBS for 10 min at 4^0 C, washed three times with PBS, permeabilized with 0.1% triton X-100 in PBS-Tween (PBST) for 30 min at room temperature, and blocked with 2% BSA in PBST for 30 min. Incubation with Asef or HA-tag antibodies were performed in blocking solution (2% BSA in PBST) for 1 hour at room temperature

followed by staining with Alexa 488-conjugated secondary antibodies. Actin filaments were stained with Texas Red-conjugated phalloidin. After immunostaining, slides were analyzed using a Nikon video imaging system (Nikon Instech Co., Japan) as described elsewhere (Birukov et al., 2004; Birukova et al., 2004b).

Differential protein fractionation and immunoblotting. Confluent HPAEC were stimulated with HGF; cytosolic and membrane fractions were isolated using a subcellular protein fractionation kit (Thermo Fisher Scientific, Rockford, IL) according to manufacturer protocol. Asef and cortactin membrane translocation was evaluated by western blot detection of changes in protein content in equal volumes of membrane fractions obtained from control and HGF-stimulated cells. For analysis of protein phosphorylation profile, cells were stimulated, then lysed, and protein extracts were separated by SDS-PAGE, transferred to polyvinylidene fluoride membrane, and probed with specific antibodies. Equal protein loading was verified by probing of membranes with antibody to β-actin or a specific protein of interest.

Permeability measurements. Endothelial permeability to macromolecules was monitored by express permeability testing assay (XPerT) recently developed in our group (Dubrovskyi et al., 2013) and now available from Millipore (Vascular Permeability Imaging Assay, cat. #17-10398). This assay is based on high affinity binding of cell impermeable avidin-conjugated FITC-labeled tracer to the

biotinylated extracellular matrix proteins immobilized on the bottom of culture dishes covered with EC monolayers. FITC-avidin binding to the matrix-coated culture dish bottoms increases if the EC barrier is compromised by treatment with a barrier-disruptive agonist. In permeability visualization experiments, 15 min after EC stimulation with HGF, FITC-avidin solution was added directly to the culture medium for 3 min before termination of the experiment. Unbound FITC-avidin was washed out with PBS (pH 7.4, 37°C), cells were fixed with 3.7% formaldehyde in PBS (10 min, room temperature) and visualization of FITC-avidin on the bottoms of coverslips was performed using the Nikon imaging system Eclipse TE 300 (Nikon, Tokyo, Japan) equipped with a digital camera (DKC 5000, Sony, Tokyo, Japan); 10× objective lenses were used. Images were processed with Adobe Photoshop 7.0 software (Adobe Systems, San Jose, CA). Measurements of transendothelial electrical resistance (TER) across confluent HPAEC monolayers were performed using the electrical cell-substrate impedance sensing system (ECIS) (Applied Biophysics, Troy, NY) as previously described (Birukov et al., 2004; Birukova et al., 2004a).

Mechanical ventilation protocol. All experimental protocols involving the use of animals were approved by the University of Chicago Institutional Animal Care & Use Committee for the humane treatment of experimental animals. Generation of *Asef-/-* mice is described elsewhere (Kawasaki et al., 2011). C57Bl-6J *Asef-/-* mice and matching controls (8-10 weeks old, males) with average weight 20-25 grams were anesthetized with an intraperitoneal injection of ketamine (75 mg/kg)

and acepromazine (1.5 mg/kg) and subjected to mechanical ventilation with high tidal volume as previously described (Birukova et al., 2010; Birukova et al., 2011). Briefly, tracheotomy was performed and the trachea was cannulated with a 20-gauge one inch catheter which was tied into place to prevent air leak. The animals were then placed on a mechanical ventilator (Harvard Apparatus, Boston, MA). Mice were randomized to concurrently receive sterile saline solution or HGF (500 μg/kg, intravenous administration) prior to a single dose of TRAP6 (1.5×10^{-5} mol/kg, intratracheal instillation) followed by 4 hours of mechanical ventilation with high tidal volume (30 ml/kg, 75 breaths per minute and 0 PEEP, HTV). Control animals were anesthetized and allowed to breathe spontaneously.

Evaluation of lung injury parameters. After the experiment, BAL was performed using 1 ml of sterile Hanks Balanced Saline Buffer. The BAL protein concentration was determined by BCATM Protein Assay kit (Thermo Scientific, Pittsburg, PA). BAL inflammatory cell counting was performed using a standard hemacytometer technique (Birukova et al., 2007b; Fu et al., 2009). Total lung myeloperoxidase (MPO) content was determined from homogenized lungs as described elsewhere (Meliton et al., 2013). For analysis of TRAP6/HTV-induced lung vascular leak, Evans blue dye (30 ml/kg) was injected into the external jugular vein 2 hours before termination of the experiment. Measurement of Evans blue accumulation in the lung tissue was performed by spectrofluorimetric analysis of lung tissue lysates according to the protocol described previously

(Moitra et al., 2007; Nonas et al., 2008). For histological assessment of lung injury, the lungs were harvested without lavage collection and fixed in 10% formaldehyde. After fixation, the lungs were embedded in paraffin, cut into 5-µm sections, and stained with hematoxylin and eosin. Sections were evaluated at 40x magnification.

Statistical analysis. Results are expressed as mean ± SD of three to six independent experiments. Stimulated samples were compared to controls by unpaired Student's *t*-tests. For multiple-group comparisons, a two-way variance analysis (ANOVA) followed by Tukey post-hoc test were used. $P<0.05$ was considered statistically significant.

AKNOWLEDGEMENTS

This work was supported by grants from National Heart, Lung, and Blood Institutes (HL89257 and HL107920) for AB and Grants-in-Aid for Scientific Research on Innovative Areas (Integrative Research on Cancer Microenvironment Network), MEXT, Japan for TA.

The authors wish to thank Katalin Szaszi (St. Michael's Hospital, Toronto, Canada) for sharing the RacG15A construct.

REFERENCES

2000. Ventilation with lower tidal volumes as compared with traditional tidal volumes for acute lung injury and the acute respiratory distress syndrome.

The Acute Respiratory Distress Syndrome Network. *N Engl J Med*. 342:1301-8.

Ammer, A.G., and S.A. Weed. 2008. Cortactin branches out: roles in regulating protrusive actin dynamics. *Cell Motil Cytoskeleton*. 65:687-707.

Anastasiadis, P.Z., S.Y. Moon, M.A. Thoreson, D.J. Mariner, H.C. Crawford, Y. Zheng, and A.B. Reynolds. 2000. Inhibition of RhoA by p120 catenin. *Nat Cell Biol*. 2:637-44.

Arthur, W.T., N.K. Noren, and K. Burridge. 2002. Regulation of Rho family GTPases by cell-cell and cell-matrix adhesion. *Biol Res*. 35:239-46.

Baumer, Y., V. Spindler, R.C. Werthmann, M. Bunemann, and J. Waschke. 2009. Role of Rac 1 and cAMP in endothelial barrier stabilization and thrombin-induced barrier breakdown. *J Cell Physiol*. 220:716-26.

Birukov, K.G., V.N. Bochkov, A.A. Birukova, K. Kawkitinarong, A. Rios, A. Leitner, A.D. Verin, G.M. Bokoch, N. Leitinger, and J.G. Garcia. 2004. Epoxycyclopentenone-containing oxidized phospholipids restore endothelial barrier function via Cdc42 and Rac. *Circ Res*. 95:892-901.

Birukov, K.G., N. Zebda, and A.A. Birukova. 2013. Barrier enhancing signals in pulmonary edema. *Compr Physiol*. 3:429-84.

Birukova, A.A., E. Alekseeva, A. Mikaelyan, and K.G. Birukov. 2007a. HGF attenuates thrombin-induced permeability in the human pulmonary endothelial cells by Tiam1-mediated activation of the Rac pathway and by Tiam1/Rac-dependent inhibition of the Rho pathway. *FASEB J*. 21:2776-86.

Birukova, A.A., K.G. Birukov, K. Smurova, D.M. Adyshev, K. Kaibuchi, I. Alieva, J.G. Garcia, and A.D. Verin. 2004a. Novel role of microtubules in thrombin-induced endothelial barrier dysfunction. *FASEB J*. 18:1879-90.

Birukova, A.A., P. Fu, S. Chatchavalvanich, D. Burdette, O. Oskolkova, V.N. Bochkov, and K.G. Birukov. 2007b. Polar head groups are important for barrier protective effects of oxidized phospholipids on pulmonary endothelium. *Am J Physiol Lung Cell Mol Physiol*. 292:L924-35.

Birukova, A.A., P. Fu, J. Xing, B. Yakubov, I. Cokic, and K.G. Birukov. 2010. Mechanotransduction by GEF-H1 as a novel mechanism of ventilator-induced vascular endothelial permeability. *Am J Physiol Lung Cell Mol Physiol*. 298:L837-48.

Birukova, A.A., K. Smurova, K.G. Birukov, K. Kaibuchi, J.G.N. Garcia, and A.D. Verin. 2004b. Role of Rho GTPases in thrombin-induced lung vascular endothelial cells barrier dysfunction. *Microvasc Res*. 67:64-77.

Birukova, A.A., Y. Tian, O. Dubrovskyi, N. Zebda, N. Sarich, X. Tian, Y. Wang, and K.G. Birukov. 2012. VE-cadherin trans-interactions modulate Rac activation and enhancement of lung endothelial barrier by iloprost. *J Cell Physiol*. 227:3405-16.

Birukova, A.A., T. Zagranichnaya, E. Alekseeva, P. Fu, W. Chen, J.R. Jacobson, and K.G. Birukov. 2007c. Prostaglandins PGE2 and PGI2 promote endothelial barrier enhancement via PKA- and Epac1/Rap1-dependent Rac activation. *Exp Cell Res*. 313:2504-20.

Birukova, A.A., N. Zebda, I. Cokic, P. Fu, T. Wu, O. Dubrovskyi, and K.G. Birukov. 2011. p190RhoGAP mediates protective effects of oxidized phospholipids in the models of ventilator-induced lung injury. *Exp Cell Res*. 317:859-72.

Bishop, A.L., and A. Hall. 2000. Rho GTPases and their effector proteins. *Biochem J*. 348 Pt 2:241-55.

Blank, R., and L.M. Napolitano. 2011. Epidemiology of ARDS and ALI. *Crit Care Clin*. 27:439-58.

Boguski, M.S., and F. McCormick. 1993. Proteins regulating Ras and its relatives. *Nature*. 366:643-54.

Borisy, G.G., and T.M. Svitkina. 2000. Actin machinery: pushing the envelope. *Curr Opin Cell Biol*. 12:104-12.

Cheng, H.T., I.P. Juang, L.C. Chen, L.Y. Lin, and C.H. Chao. 2013. Association of Asef and Cdc42 expression to tubular injury in diseased human kidney. *J Investig Med*. 61:1097-103.

Date, I., N. Takagi, K. Takagi, T. Kago, K. Matsumoto, T. Nakamura, and S. Takeo. 2004. Hepatocyte growth factor attenuates cerebral ischemia-induced learning dysfunction. *Biochem Biophys Res Commun*. 319:1152-8.

Dubrovskyi, O., A.A. Birukova, and K.G. Birukov. 2013. Measurement of local permeability at subcellular level in cell models of agonist- and ventilator-induced lung injury. *Lab Invest*. 93:254-63.

Dudek, S.M., J.R. Jacobson, E.T. Chiang, K.G. Birukov, P. Wang, X. Zhan, and J.G. Garcia. 2004. Pulmonary endothelial cell barrier enhancement by sphingosine 1-phosphate: roles for cortactin and myosin light chain kinase. *J Biol Chem*. 279:24692-700.

Essler, M., M. Amano, H.J. Kruse, K. Kaibuchi, P.C. Weber, and M. Aepfelbacher. 1998. Thrombin inactivates myosin light chain phosphatase via Rho and its target Rho kinase in human endothelial cells. *J Biol Chem*. 273:21867-74.

Finigan, J.H., S.M. Dudek, P.A. Singleton, E.T. Chiang, J.R. Jacobson, S.M. Camp, S.Q. Ye, and J.G. Garcia. 2005. Activated protein C mediates novel lung endothelial barrier enhancement: role of sphingosine 1-phosphate receptor transactivation. *J Biol Chem*. 280:17286-93.

Fu, P., A.A. Birukova, J. Xing, S. Sammani, J.S. Murley, J.G. Garcia, D.J. Grdina, and K.G. Birukov. 2009. Amifostine reduces lung vascular permeability via suppression of inflammatory signalling. *Eur Respir J*. 33:612-24.

Fukuhara, S., A. Sakurai, H. Sano, A. Yamagishi, S. Somekawa, N. Takakura, Y. Saito, K. Kangawa, and N. Mochizuki. 2005. Cyclic AMP potentiates vascular endothelial cadherin-mediated cell-cell contact to enhance endothelial barrier function through an Epac-Rap1 signaling pathway. *Mol Cell Biol*. 25:136-46.

Garcia-Mata, R., K. Wennerberg, W.T. Arthur, N.K. Noren, S.M. Ellerbroek, and K. Burridge. 2006. Analysis of activated GAPs and GEFs in cell lysates. *Methods Enzymol*. 406:425-37.

Garcia, J.G., F. Liu, A.D. Verin, A. Birukova, M.A. Dechert, W.T. Gerthoffer, J.R. Bamberg, and D. English. 2001. Sphingosine 1-phosphate promotes endothelial cell barrier integrity by Edg-dependent cytoskeletal rearrangement. *J Clin Invest*. 108:689-701.

Geiser, T. 2003. Mechanisms of alveolar epithelial repair in acute lung injury--a translational approach. *Swiss Med Wkly*. 133:586-90.

Head, J.A., D. Jiang, M. Li, L.J. Zorn, E.M. Schaefer, J.T. Parsons, and S.A. Weed. 2003. Cortactin tyrosine phosphorylation requires Rac1 activity and association with the cortical actin cytoskeleton. *Mol Biol Cell*. 14:3216-29.

Kawasaki, Y., S. Furukawa, R. Sato, and T. Akiyama. 2013. Differences in the localization of the adenomatous polyposis coli-Asef/Asef2 complex between adenomatous polyposis coli wild-type and mutant cells. *Cancer Sci*. 104:1135-8.

Kawasaki, Y., T. Jigami, S. Furukawa, M. Sagara, K. Echizen, Y. Shibata, R. Sato, and T. Akiyama. 2011. The adenomatous polyposis coli-associated guanine nucleotide exchange factor Asef is involved in angiogenesis. *J Biol Chem*. 285:1199-207.

Kawasaki, Y., R. Sato, and T. Akiyama. 2003. Mutated APC and Asef are involved in the migration of colorectal tumour cells. *Nat Cell Biol*. 5:211-5.

Kawasaki, Y., T. Senda, T. Ishidate, R. Koyama, T. Morishita, Y. Iwayama, O. Higuchi, and T. Akiyama. 2000. Asef, a link between the tumor suppressor APC and G-protein signaling. *Science*. 289:1194-7.

Kawasaki, Y., S. Tsuji, M. Sagara, K. Echizen, Y. Shibata, and T. Akiyama. 2009. Adenomatous polyposis coli and Asef function downstream of hepatocyte growth factor and phosphatidylinositol 3-kinase. *J Biol Chem*. 284:22436-43.

Liu, F., K.L. Schaphorst, A.D. Verin, K. Jacobs, A. Birukova, R.M. Day, N. Bogatcheva, D.P. Bottaro, and J.G. Garcia. 2002. Hepatocyte growth factor enhances endothelial cell barrier function and cortical cytoskeletal rearrangement: potential role of glycogen synthase kinase-3beta. *FASEB J*. 16:950-62.

Matsumoto, K., and T. Nakamura. 1996. Emerging multipotent aspects of hepatocyte growth factor. *J Biochem (Tokyo)*. 119:591-600.

Matthay, M.A., G.A. Zimmerman, C. Esmon, J. Bhattacharya, B. Coller, C.M. Doerschuk, J. Floros, M.A. Gimbrone, Jr., E. Hoffman, R.D. Hubmayr, M. Leppert, S. Matalon, R. Munford, P. Parsons, A.S. Slutsky, K.J. Tracey, P. Ward, D.B. Gail, and A.L. Harabin. 2003. Future research directions in acute lung injury: summary of a National Heart, Lung, and Blood Institute working group. *Am J Respir Crit Care Med*. 167:1027-35.

Meliton, A.Y., N.M. Munoz, L.N. Meliton, A.A. Birukova, A.R. Leff, and K.G. Birukov. 2013. Mechanical induction of group V phospholipase A(2) causes lung inflammation and acute lung injury. *Am J Physiol Lung Cell Mol Physiol*. 304:L689-700.

Moitra, J., S. Sammani, and J.G. Garcia. 2007. Re-evaluation of Evans Blue dye as a marker of albumin clearance in murine models of acute lung injury. *Transl Res*. 150:253-65.

Nimnual, A.S., L.J. Taylor, and D. Bar-Sagi. 2003. Redox-dependent downregulation of Rho by Rac. *Nat Cell Biol*. 5:236-41.

Nonas, S., A.A. Birukova, P. Fu, J. Xing, S. Chatchavalvanich, V.N. Bochkov, N. Leitinger, J.G. Garcia, and K.G. Birukov. 2008. Oxidized phospholipids reduce ventilator-induced vascular leak and inflammation in vivo. *Crit Care*. 12:R27.

Noren, N.K., C.M. Niessen, B.M. Gumbiner, and K. Burridge. 2001. Cadherin engagement regulates Rho family GTPases. *J Biol Chem*. 276:33305-8.

Poh, Y.C., S. Na, F. Chowdhury, M. Ouyang, Y. Wang, and N. Wang. 2009. Rapid activation of Rac GTPase in living cells by force is independent of Src. *PLoS One*. 4:e7886.

Quesnel, C., S. Marchand-Adam, A. Fabre, J. Marchal-Somme, I. Philip, S. Lasocki, V. Lecon, B. Crestani, and M. Dehoux. 2008. Regulation of hepatocyte growth factor secretion by fibroblasts in patients with acute lung injury. *Am J Physiol Lung Cell Mol Physiol*. 294:L334-43.

Servitja, J.M., M.J. Marinissen, A. Sodhi, X.R. Bustelo, and J.S. Gutkind. 2003. Rac1 function is required for Src-induced transformation. Evidence of a role for Tiam1 and Vav2 in Rac activation by Src. *J Biol Chem*. 278:34339-46.

Singleton, P.A., R. Salgia, L. Moreno-Vinasco, J. Moitra, S. Sammani, T. Mirzapoiazova, and J.G. Garcia. 2007. CD44 regulates hepatocyte growth factor-mediated vascular integrity. Role of c-Met, Tiam1/Rac1, dynamin 2, and cortactin. *J Biol Chem*. 282:30643-57.

Stern, J.B., L. Fierobe, C. Paugam, C. Rolland, M. Dehoux, A. Petiet, M.C. Dombret, J. Mantz, M. Aubier, and B. Crestani. 2000. Keratinocyte growth factor and hepatocyte growth factor in bronchoalveolar lavage fluid in acute respiratory distress syndrome patients. *Crit Care Med*. 28:2326-33.

Storck, J., and E.R. Zimmermann. 1996. Regulation of the thrombin receptor response in human endothelial cells. *Thromb Res*. 81:121-31.

Stultiens, A., T.T. Ho, B.V. Nusgens, A.C. Colige, and C.F. Deroanne. 2012. Rho proteins crosstalk via RhoGDIalpha: At random or hierarchically ordered? *Commun Integr Biol*. 5:99-101.

Tauseef, M., V. Kini, N. Knezevic, M. Brannan, R. Ramchandaran, H. Fyrst, J. Saba, S.M. Vogel, A.B. Malik, and D. Mehta. 2008. Activation of sphingosine kinase-1 reverses the increase in lung vascular permeability through sphingosine-1-phosphate receptor signaling in endothelial cells. *Circ Res*. 103:1164-72.

Tian, Y., X. Tian, G. Gawlak, J.J. O'Donnell, 3rd, D.B. Sacks, and A.A. Birukova. 2014. IQGAP1 regulates endothelial barrier function via EB1 - cortactin crosstalk. *Mol Cell Biol*. 34:3546-58.

Uruno, T., J. Liu, P. Zhang, Y. Fan, C. Egile, R. Li, S.C. Mueller, and X. Zhan. 2001. Activation of Arp2/3 complex-mediated actin polymerization by cortactin. *Nat Cell Biol*. 3:259-66.

Velasco, G., C. Armstrong, N. Morrice, S. Frame, and P. Cohen. 2002. Phosphorylation of the regulatory subunit of smooth muscle protein phosphatase 1M at Thr850 induces its dissociation from myosin. *FEBS Lett*. 527:101-4.

Verghese, G.M., K. McCormick-Shannon, R.J. Mason, and M.A. Matthay. 1998. Hepatocyte growth factor and keratinocyte growth factor in the pulmonary edema fluid of patients with acute lung injury. Biologic and clinical significance. *Am J Respir Crit Care Med*. 158:386-94.

Vouret-Craviari, V., C. Bourcier, E. Boulter, and E. van Obberghen-Schilling. 2002. Distinct signals via Rho GTPases and Src drive shape changes by thrombin and sphingosine-1-phosphate in endothelial cells. *J Cell Sci*. 115:2475-84.

Waheed, F., Q. Dan, Y. Amoozadeh, Y. Zhang, S. Tanimura, P. Speight, A. Kapus, and K. Szaszi. 2013. Central role of the exchange factor GEF-H1 in TNF-alpha-induced sequential activation of Rac, ADAM17/TACE, and RhoA in tubular epithelial cells. *Mol Biol Cell*. 24:1068-82.

Ware, L.B., and M.A. Matthay. 2002. Keratinocyte and hepatocyte growth factors in the lung: roles in lung development, inflammation, and repair. *Am J Physiol Lung Cell Mol Physiol*. 282:L924-40.

Weed, S.A., Y. Du, and J.T. Parsons. 1998. Translocation of cortactin to the cell periphery is mediated by the small GTPase Rac1. *J Cell Sci*. 111:2433-43.

Weed, S.A., and J.T. Parsons. 2001. Cortactin: coupling membrane dynamics to cortical actin assembly. *Oncogene*. 20:6418-34.

Welch, H.C., W.J. Coadwell, L.R. Stephens, and P.T. Hawkins. 2003. Phosphoinositide 3-kinase-dependent activation of Rac. *FEBS Lett*. 546:93-7.

Zebda, N., Y. Tian, X. Tian, G. Gawlak, K. Higginbotham, A.B. Reynolds, A.A. Birukova, and K.G. Birukov. 2013. Interaction of p190RhoGAP with C-terminal domain of p120-catenin modulates endothelial cytoskeleton and permeability *J Biol Chem*. 288:18290-9.

Zheng, Y. 2001. Dbl family guanine nucleotide exchange factors. *Trends Biochem Sci*. 26:724-32.

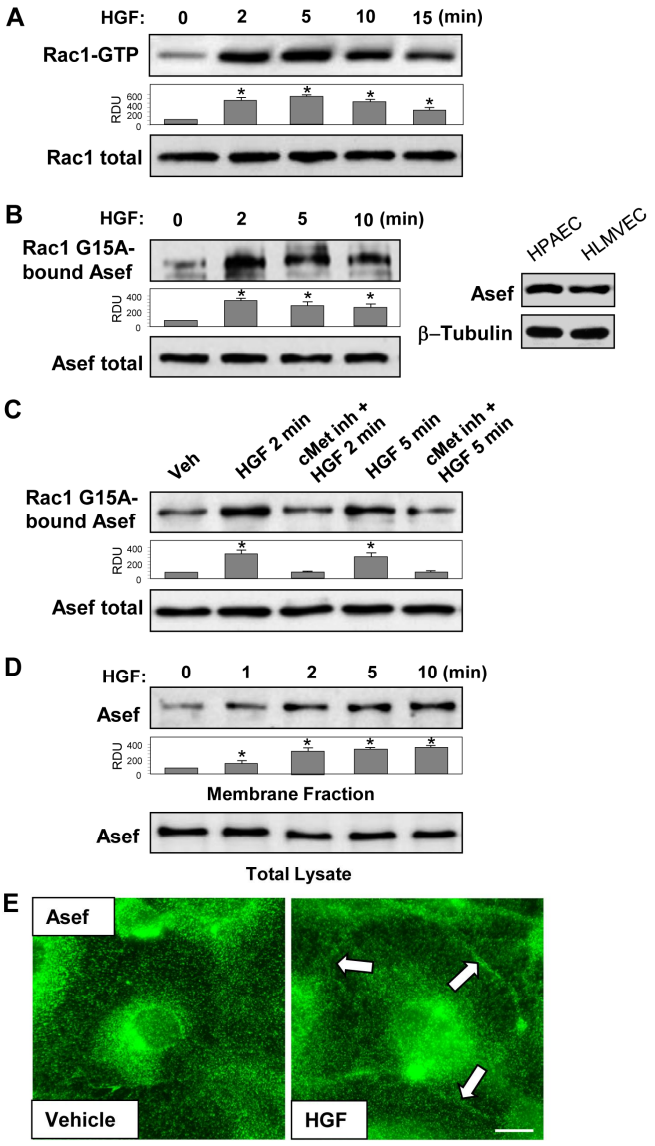

Figure 1. HGF induces activation of Asef and Rac1. A - D: HPAEC were stimulated with HGF (50 ng/ml) for the indicated periods of time. **A:** Rac1 activation was determined by Rac-GTP pulldown assay. Content of activated

Rac1 was normalized to the total Rac1 content in EC lysates. *P <0.05 vs. vehicle. **B:** Asef activation was determined by pulldown assay with immobilized Rac1G15A and evaluated by increased Asef association with Rac1G15A. Content of activated Asef was normalized to the total Asef content in EC lysates. *P <0.05 vs. vehicle. **C:** HPAEC were preincubated with vehicle or c-Met inhibitor (carboxamide 50 nM, 30 min) followed by stimulation with HGF (2 min and 5 min). Asef activation was determined by pulldown assay with immobilized Rac1G15A and normalized to the total Asef. *P <0.05 vs. cMet inh + HGF. **D:** HPAEC were stimulated with HGF followed by isolation of cytosolic and membrane fractions. Time dependent, HGF-induced accumulation of Asef in membrane fraction was detected with specific antibodies. Asef content in corresponding total cell lysates was used as a normalization control. *P <0.05 vs. vehicle. **D:** Endothelial cells grown on glass coverslips were stimulated with HGF (50 ng/ml, 30 min). Intracellular redistribution of endogenous Asef was examined by immunofluorescence staining with Asef antibody. Shown are representative results of three to five independent experiments. Bar=5 μm.

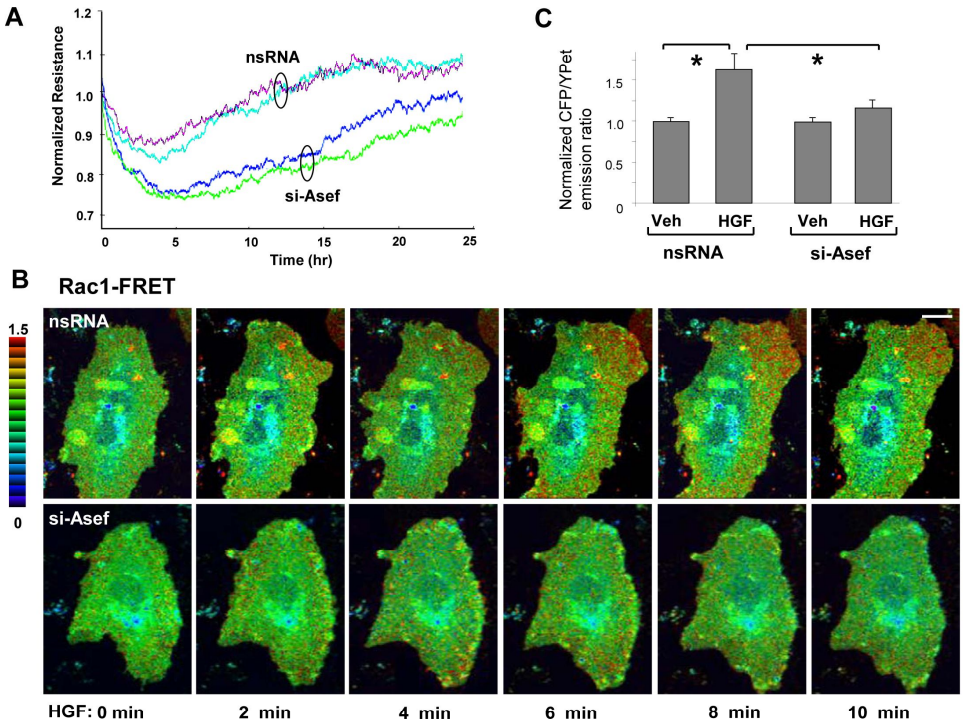
A
Normalized Resistance
1.2
1.1
1.0
0.9
0.8
0.7
nsRNA
si-Asef
0
5
10
15
20
25
Time (hr)
C
Normalized CFP/YPet emission ratio
1.5
1.0
0.5
0
*
*
Veh
HGF
Veh
HGF
nsRNA
si-Asef
B
Rac1-FRET
1.5
0
nsRNA
si-Asef
HGF: 0 min
2 min
4 min
6 min
8 min
10 min

Tian et al., Figure 2DEF

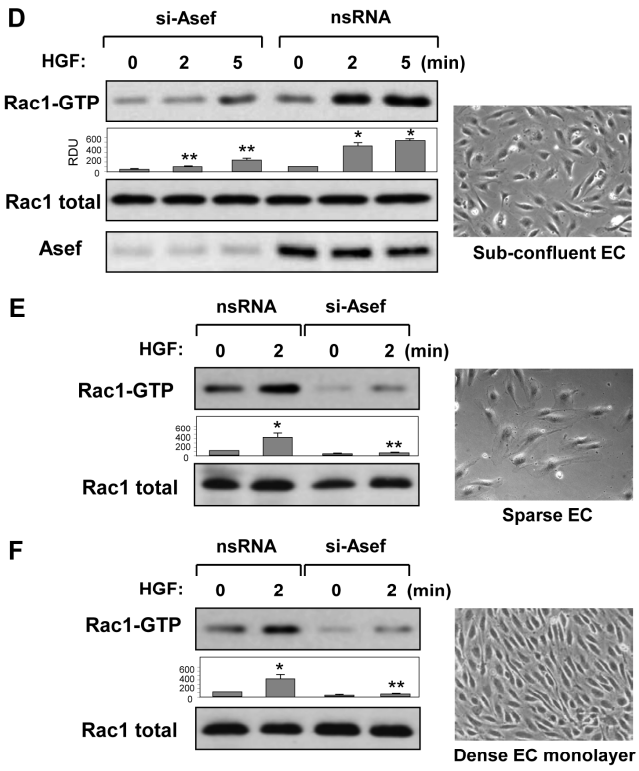

Figure 2. Asef knockdown attenuates HGF-induced Rac1 activation. A: Endothelial cells were transfected with control or 100 nM Asef-specific siRNA, and after 24 hrs changes in TER were monitored over time. **B:** FRET analysis of

HGF-induced Rac1 activation. HPAEC were transfected with non-specific or Asef-specific siRNA duplexes for 24 hr followed by transfection with CFP/YPet-Rac1 biosensor for additional 24 hrs. FRET analysis of time-dependent Rac activation was performed in HGF-stimulated control and Asef knockdown cells. Images represent a ratio of activated Rac1 to the total Rac1 content. Areas of Rac1 activation appear in red. Bar=5 μm. **C:** Quantitative analysis of HGF-induced Rac1 activation at the cell periphery. Bar graphs represent normalized CFP/YPet emission ratio. Rac1 activation in cells prior to HGF stimulation was compared to Rac1 activation after 6 min of HGF addition. Data are expressed as mean ± SD of four independent experiments, 5-7 cells for each experiment; *p<0.05. **D-F:** Sub-confluent (**D**), sparse (**E**), or dense (**F**) HPAEC were transfected with Asef-specific siRNA or non-specific RNA and stimulated with HGF (50 ng/ml). **Left panels:** Rac1 activation was determined by Rac-GTP pulldown assay. The content of activated Rac1 was normalized to the total Rac1 content in EC lysates. *P <0.01 vs. non-stimulated cells treated with non-specific (ns) RNA; **P <0.01 vs. nsRNA. **Right panels:** Representative phase-contrast images of HPAEC used for experiments.

Tian et al., Figure 3AB

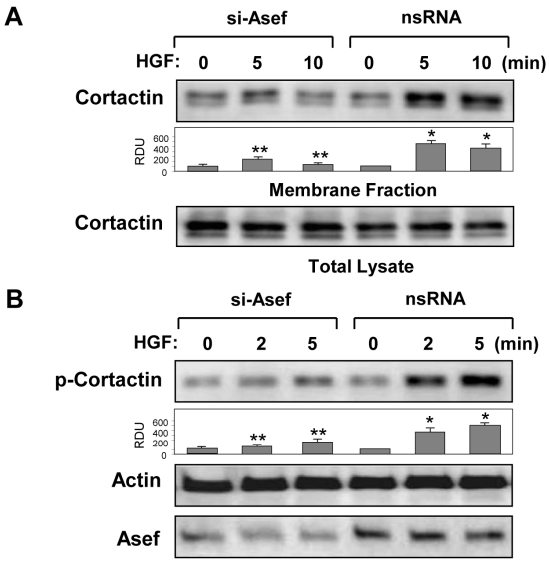

Tian et al., Figure 3C

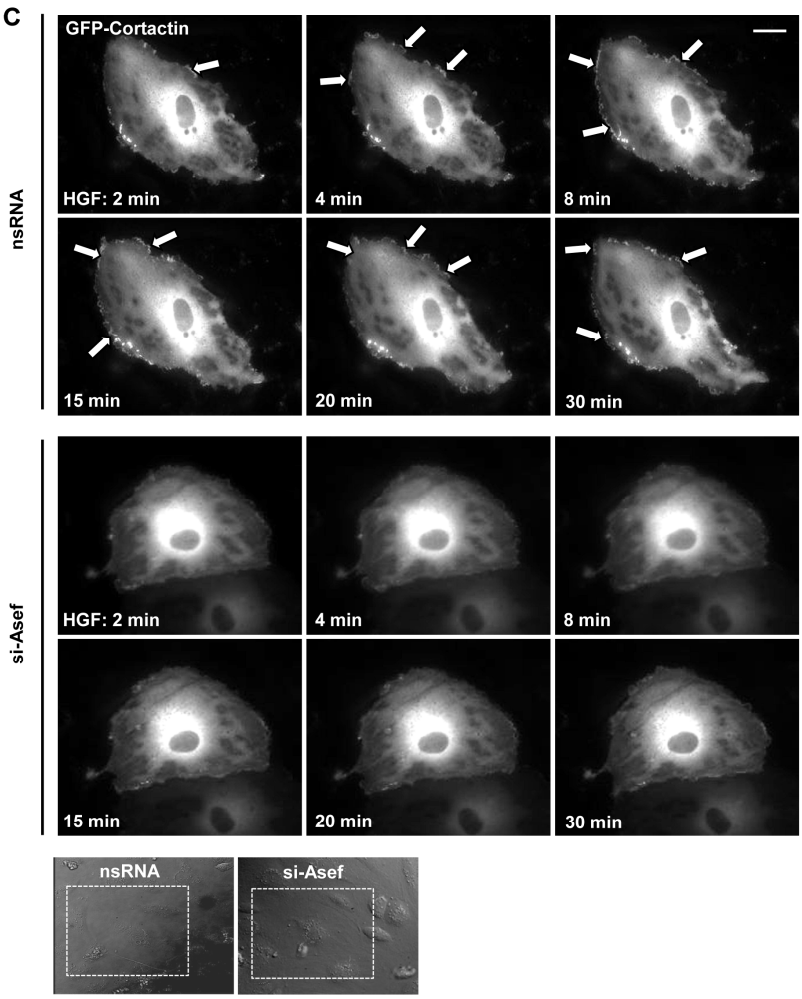

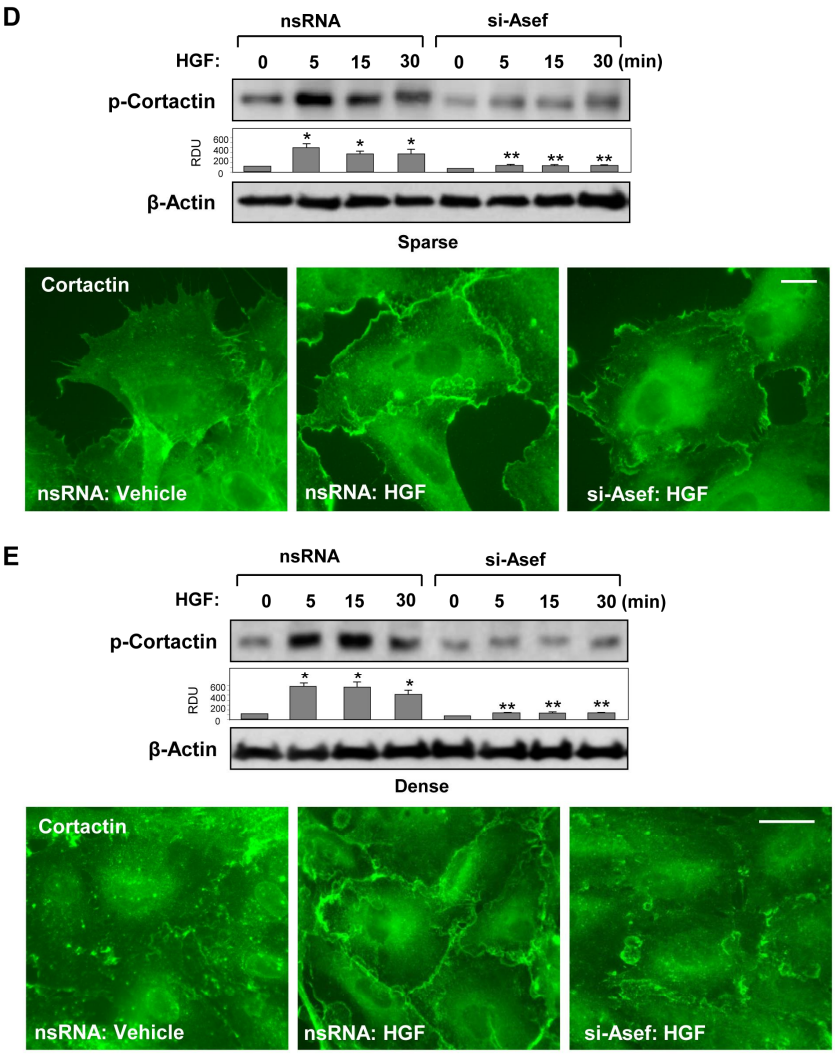

Figure 3. Asef knockdown attenuates HGF-induced cortactin activation. HPAEC were transfected with Asef-specific siRNA or non-specific RNA and stimulated with HGF (50 ng/ml). **A:** After isolation of cytosolic and membrane

fractions, cortactin accumulation in membrane fraction was monitored by western blot. Cortactin content in corresponding total cell lysates was used as a normalization control. **B:** Effect of Asef knockdown on HGF-induced cortactin phosphorylation was evaluated by western blot with phospho-Tyr^{421}-cortactin antibody. Equal protein loading was confirmed by membrane probing with β-actin antibody. siRNA-induced Asef protein depletion was confirmed by western blot analysis of whole cell lysates. *P <0.01 vs. non-stimulated cells treated with nsRNA; **P <0.01 vs. nsRNA. **C:** Live cell imaging of HPAEC transfected with Asef siRNA or nonspecific RNA and expressing GFP- cortactin. Snapshots depict HGF-induced cortical dynamics at cell periphery of control and Asef-depleted cells. Bar=5 μm. **D and E:** Effect of Asef knockdown on HGF-induced cortactin phosphorylation in sparse (**D,** bar = 5 μm) or dense (**E,** bar = 10 μm) HPAEC culture was evaluated by western blot with phospho-Tyr^{421}-cortactin antibody. Equal protein loading was confirmed by membrane probing with β-actin antibody. *P <0.01 vs. non-stimulated cells treated with nsRNA; **P <0.01 vs. nsRNA. HGF-induced cortactin translocation was evaluated by immunofluorescence staining of formaldehyde-fixed EC. Results are representative of three independent experiments.

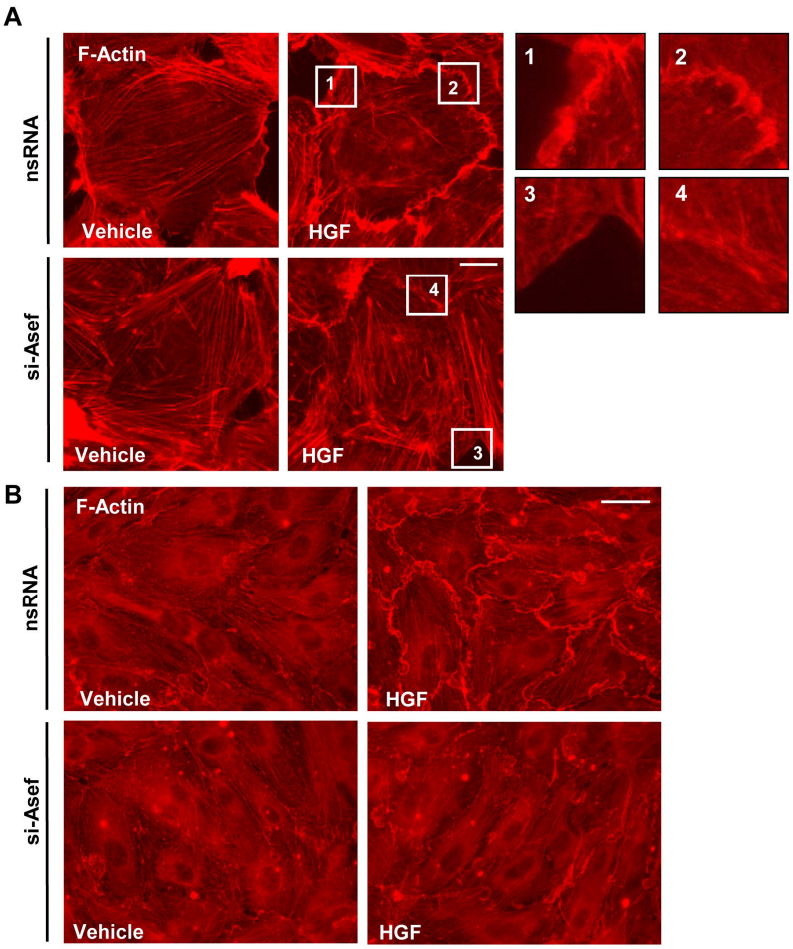
A
nsRNA
si-Asef
F-Actin
Vehicle
HGF
1
2
3
4
B
nsRNA
si-Asef
F-Actin
Vehicle
HGF

Tian et al., Figure 4CD

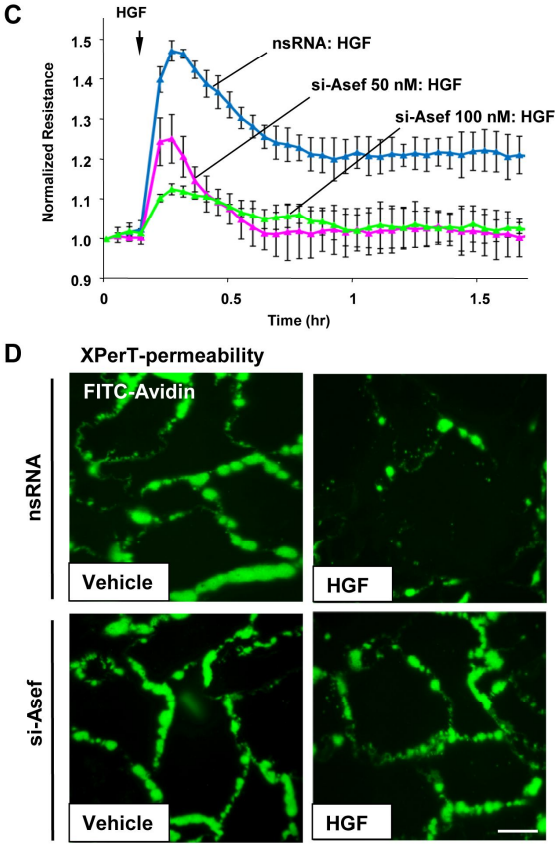

Figure 4. Asef knockdown attenuates HGF-induced peripheral actin remodeling and EC barrier enhancement. A and B: Control and Asef-depleted EC were stimulated with HGF (50 ng/ml, 10 min). Immunofluorescence

visualization of actin cytoskeleton was performed in subconfluent (**A,** bar = 5 µm) or dense (**B,** bar = 10 µm) EC culture using TR-phalloidin staining. HGF-induced peripheral accumulation of polymerized actin was abolished by Asef knockdown. Magnified images **(insets)** show details of actin structure. **C:** Permeability measurements. Control and Asef-depleted EC were stimulated with HGF (50 ng/ml), and TER was monitored over time. Shown are cumulative data of five independent experiments. Results are represented as mean ± SD. **D:** HPAEC grown on glass coverslips with immobilized biotinylated gelatin (0.25 mg/ml) and transfected with Asef-specific siRNA or non-specific RNA and then stimulated with vehicle or HGF (50 ng/ml, 10 min) followed by addition of FITC-avidin (25 µg/ml, 3 min). Unbound FITC-avidin was removed, and FITC fluorescence signal was visualized by fluorescence microscopy. Bar= 10 µm.

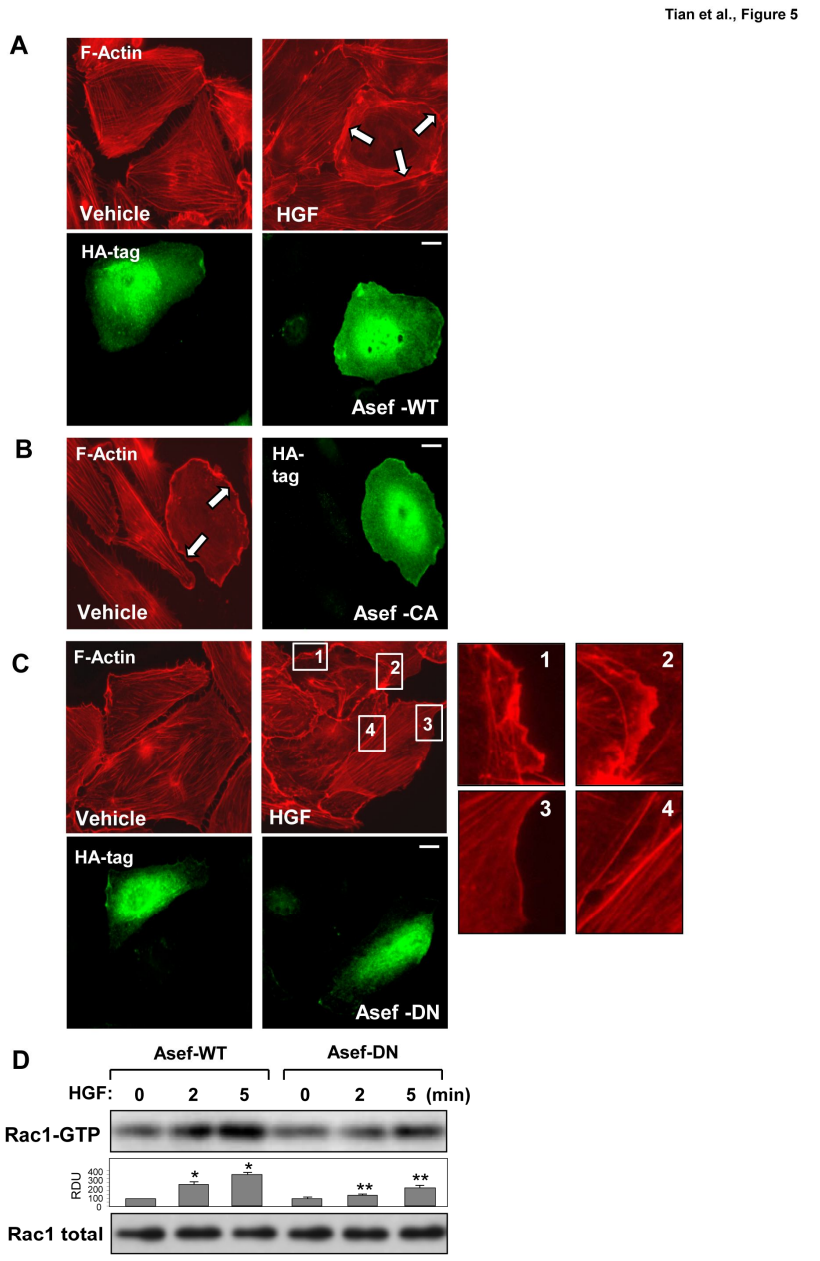

Figure 5. Role of Asef activity in HGF-induced actin remodeling. HA-tagged wild type Asef, constitutively active (CA-Asef) or dominant negative (DN-Asef)

Asef mutants were expressed in HPAEC. After stimulation with vehicle or HGF(50 ng/ml, 10 min), cells were fixed in 4.7% formaldehyde, and F-actin was visualized by Texas Red phalloidin staining. Cells expressing recombinant Asef were visualized by immunofluorescence staining for HA-tag. **A:** Cells transfected with wild type Asef were treated with vehicle or HGF. **B:** Expression of constitutively active Asef mutant (ΔAPC-Asef). **C:** Expression of dominant negative Asef mutant (ΔDH-Asef). Inset with higher magnification image of cell edge depicts inhibition of HGF-induced formation of lamellipodia-like structures by expression of dominant negative Asef mutant. Arrows show cells with activated peripheral actin cytoskeletal remodeling. Bar= 5 μm. **D:** EC monolayers were transiently transfected with wild type Asef or dominant negative Asef mutant, and HGF-induced Rac1 activation was determined by Rac-GTP pulldown assay. The content of activated Rac1 was normalized to the total Rac1 content in EC lysates; *P <0.01 vs. non-stimulated controls trasnfected with Asef-WT; **P <0.05 vs. Asef-WT.

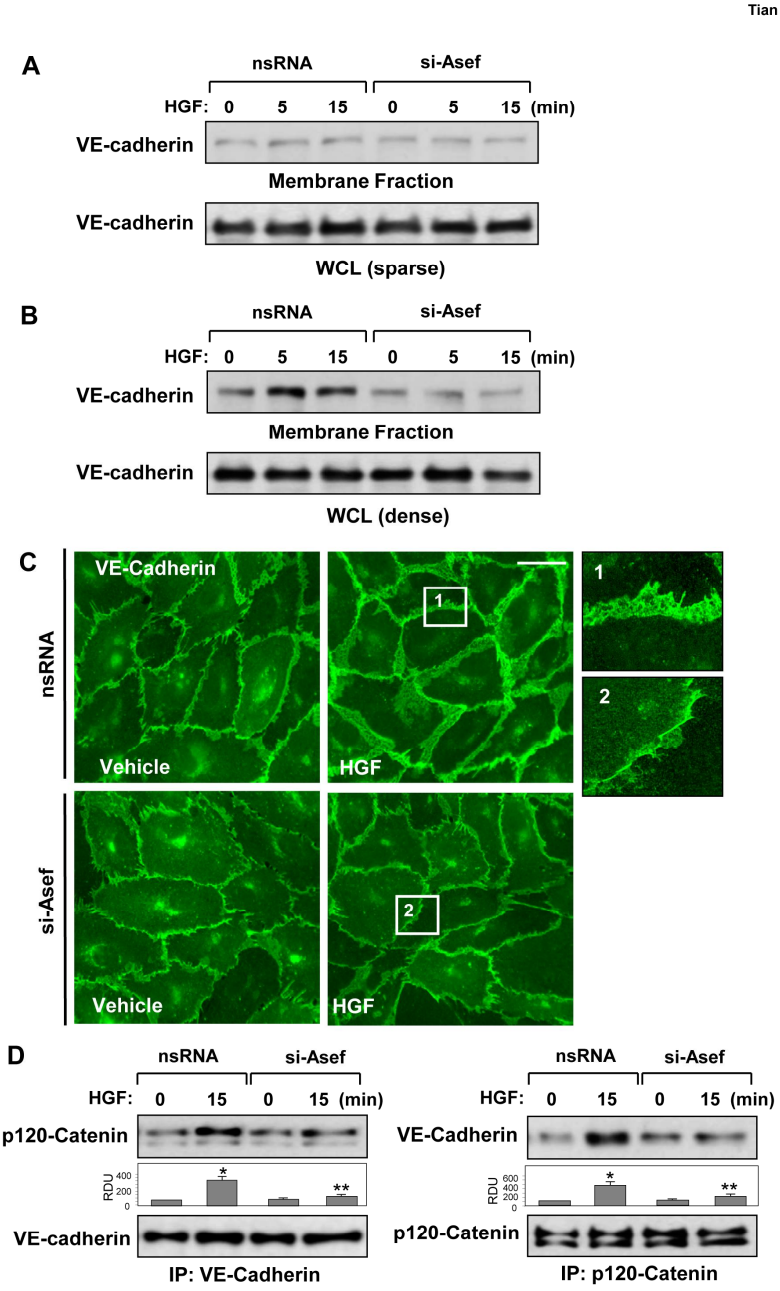

Figure 6. Asef knockdown attenuates HGF-induced enhancement of adherens junctions. HPAEC were transfected with Asef-specific siRNA or non-

specific RNA and stimulated with HGF (50 ng/ml). **A and B:** Sparse (**A**), or dense (**B**) HPAEC cultures were stimulated with HGF followed by isolation of membrane fraction. HGF-induced VE-cadherin accumulation in the membrane fraction was detected with specific antibodies. VE-cadherin content in corresponding total cell lysates was used as a normalization control. **C:** Visualization of cell-cell contacts was performed by immunofluorescence staining of formaldehyde-fixed HPAEC with VE-cadherin antibody; Bar = 10 μm. Magnified images **(insets)** show details of adherens junction structures. **D:** HGF-treated HPAEC were used for reciprocal co-immunoprecipitation assays with VE-cadherin (**upper panels**) and p120-catenin (**lower panels**) antibodies followed by western blot detection of p120-catenin and VE-cadherin; *P <0.01 vs. non-stimulated cells treated with nsRNA; **P <0.05 vs. nsRNA. Results are representative of three independent experiments.

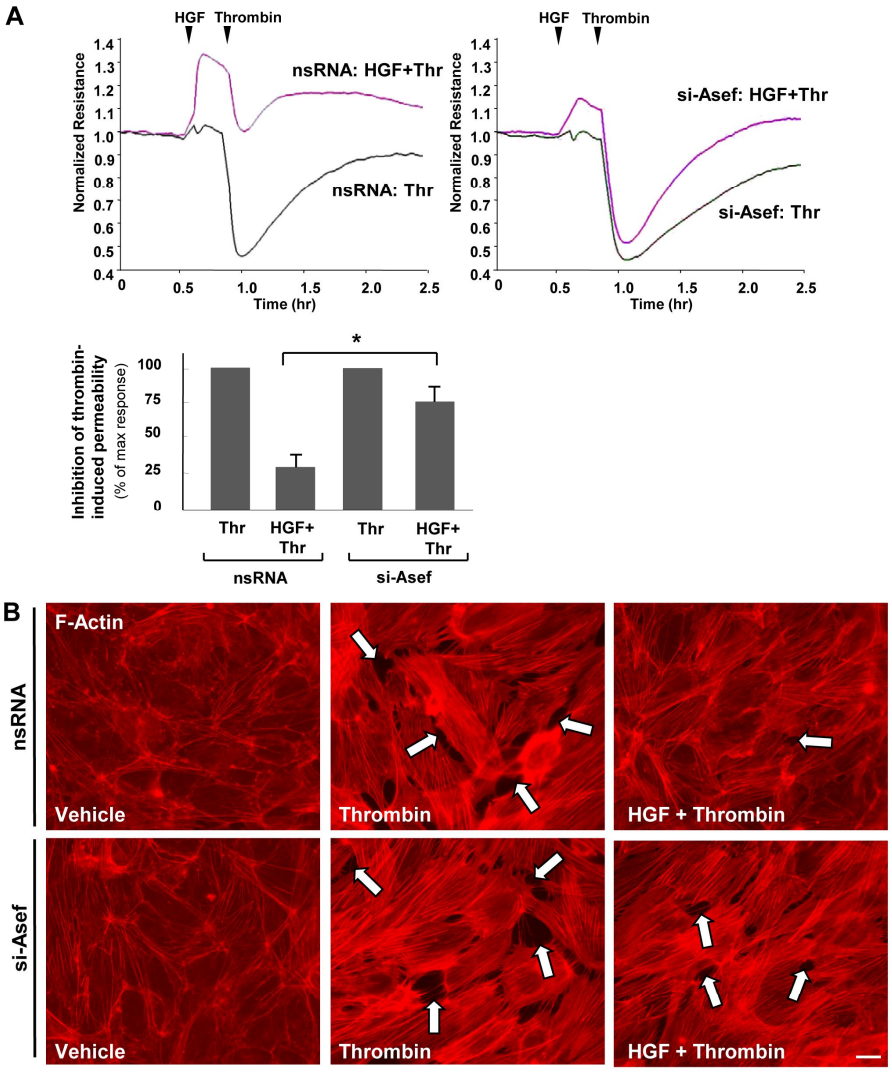
A
HGF
Thrombin
nsRNA: HGF+Thr
nsRNA: Thr
si-Asef: HGF+Thr
si-Asef: Thr
Normalized Resistance
Time (hr)
Inhibition of thrombin-induced permeability
(% of max response)
Thr
HGF+ Thr
nsRNA
si-Asef
B
F-Actin
nsRNA
si-Asef
Vehicle
Thrombin
HGF + Thrombin

Tian et al., Figure 7CD

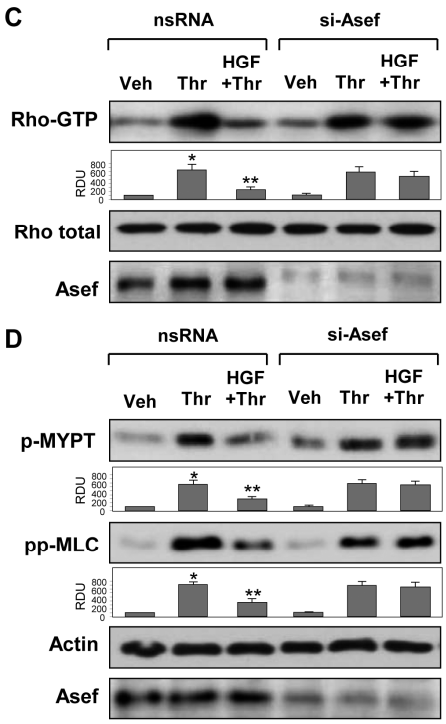

Figure 7. Asef knockdown attenuates HGF protective effects against thrombin-induced EC barrier disruption. A: Measurements of TER: Endothelial cells were transfected with 100 nM Asef-specific siRNA or non-

specific RNA 72 hrs prior to TER measurements. After 15-min pretreatment with vehicle or HGF, cells were stimulated with thrombin (0.5 U/ml, shown by arrow). The TER was monitored over time. Shown are representative data of five independent experiments. Bar graph depicts EC permeability changes at the time point corresponding to the maximal TER response. Results are represented as mean ± SD; *P<0.01. **B:** EC monolayers transfected with nonspecific RNA or Asef-specific siRNA were stimulated with thrombin (0.5 U/ml, 10 min) with or without HGF pretreatment (50 ng/ml, 15 min). Stress fiber formation and integrity of EC monolayer was monitored by immunofluorescence staining with Texas Red phalloidin. Paracellular gaps and disrupted intercellular contacts are marked by arrows. Bar=10 μm. **C:** Cells treated with nonspecific or Asef-specific siRNA were stimulated with thrombin (0.5 U/ml, 10 min) with or without HGF pretreatment (50 mg/ml, 15 min). Rho activation was evaluated by RhoGTP pulldown assay and normalized to total Rho content in cell lysates. Asef depletion was verified by western blot. **D:** Activation of Rho pathway was evaluated by western blot analysis of phospho-MYPT and diphospho-MLC levels. Reprobing with β-actin antibody was used as the normalization control. Asef depletion was verified by western blot. Bar graphs depict quantitative densitometry analysis of western blot data; *P <0.05 thrombin nsRNA vs. HGF + thrombin nsRNA; **P <0.05 HGF + thrombin; nsRNA vs. si-Asef.

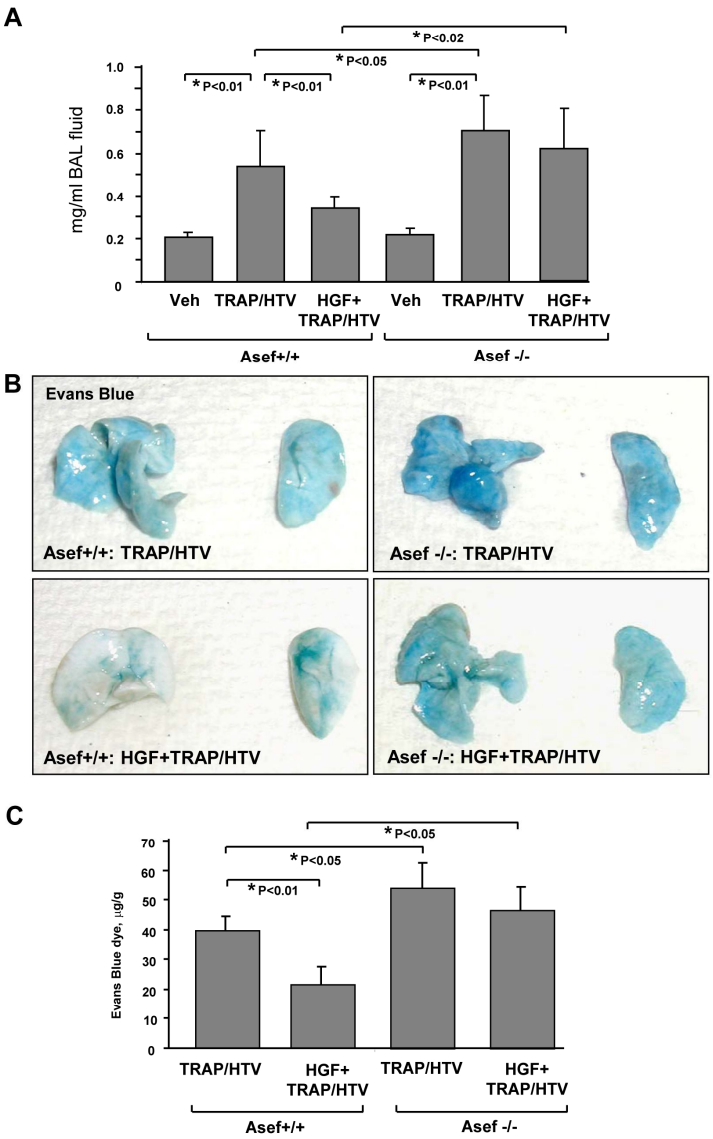

Figure 8. Role of Asef in HGF-induced lung barrier protection in the model of TRAP6/HTV-induced lung injury. *Asef*+/+ and *Asef*-/- mice were treated with

vehicle or HGF (500 µg/kg, i/v) followed by TRAP6 injection (1.5 x 10^{-5} mol/kg, i/t) and mechanical ventilation at high tidal volume (HTV, 30 ml/kg, 4 hr). **A:** Measurements of protein concentration in BAL fluid; n=6. **B:** Vascular leak was analyzed by Evans blue-labeled albumin extravasation into the lung tissue. **C:** The quantitative analysis of Evans blue labeled albumin extravasation was performed by spectrophotometric evaluation of Evans blue extracted from the lung tissue samples; n=6.

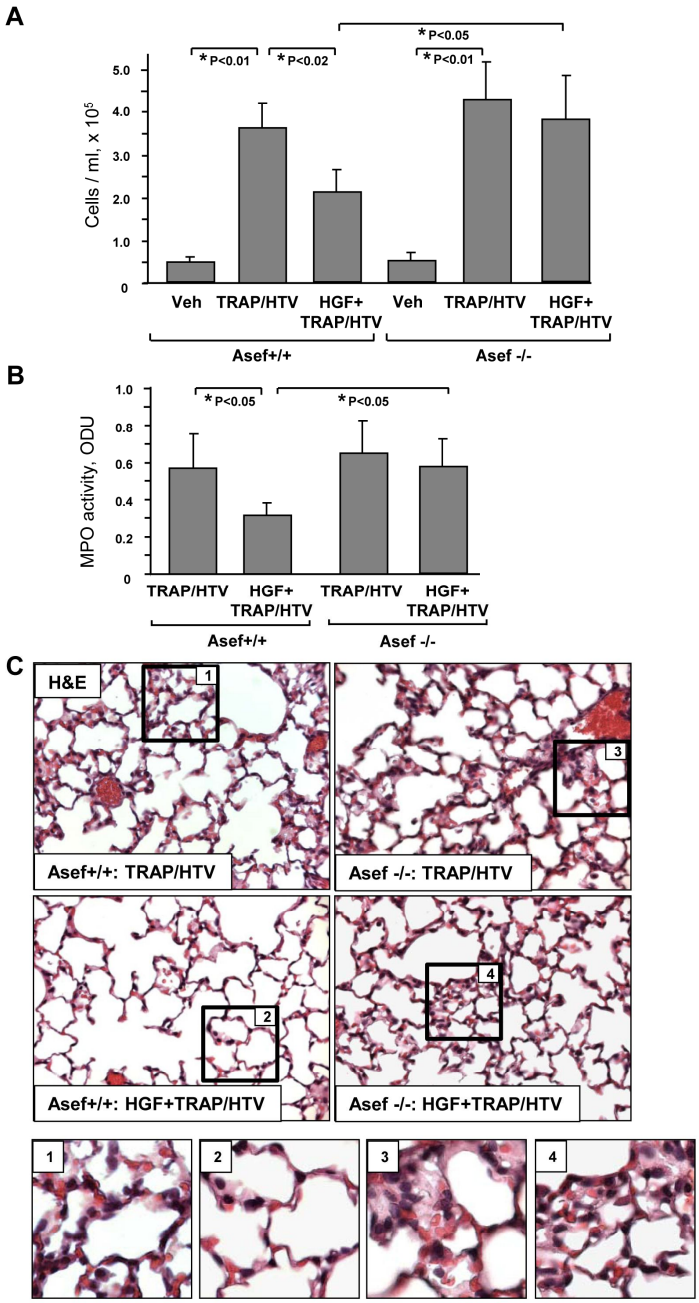

Figure 9. Role of Asef in the HGF protection against leukocyte infiltration in TRAP6/HTV-induced lung injury. *Asef*+/+ and *Asef-/-* mice were treated with

vehicle or HGF (500 µg/kg, i/v) followed by TRAP6 injection (1.5 x 10^{-5} mol/kg, i/t) and mechanical ventilation at high tidal volume (HTV, 30 ml/kg, 4 hr). **A:** Total cell count and neutrophil count was performed in BAL fluid; n=6. **B:** Measurements of myeloperoxidase (MPO) activity in lung samples from *Asef*+/+ and *Asef*-/- mice exposed to TRAP6/HTV with or without HGF pretreatment; n=4. **C:** Whole lungs were fixed in 10% formalin, and used for histological evaluation by hematoxylin and eosin staining. Images are representative of 4-6 lung specimens for each condition with ×40 magnification. **Insets:** higher magnification images of lung tissue.